euronoise

Prediction of flow induced noise in rotating devices using nonmatching grids

J. Grabinger[a], B. Karic[b], S. Triebenbacher[a], M. Kaltenbacher[a], S. Becker[b] and R. Lerch[a]

[a]Univ. Erlangen-Nuremberg, Dept. of Sensor Technology, Paul-Gordan-Str. 3/5, 91052 Erlangen, Germany
[b]University Erlangen-Nuremberg, Institute of Fluid Mechanics, Cauerst. 4, 91058 Erlangen, Germany
jens.grabinger@lse.eei.uni-erlangen.de

With increasing number of electrical devices, e.g. air conditioning systems, used in homes and offices, noise pollution is becoming a more and more relevant topic. A large amount of this noise is generated by turbulent flows and laminar flows at leading and trailing edges, where mainly tonal noise is generated. The objective of our contribution is to simulate the generation as well as the propagation of noise inside of rotating devices. The acoustic source terms are obtained from the fluid dynamics solution by using Lighthill's acoustic analogy. The acoustic domain is decomposed into a rotating part and a fixed part. The coupling between these two parts is enforced at their interface by a mortar finite element method, which uses Lagrange multipliers in order to "glue" the geometrically independent parts together. The mortar method takes into account the movement of the rotating part by a moving nonmatching grid, that is recomputed at each time step.

1 Introduction

If one wants to reduce the flow-generated noise in rotating devices — such as fans, impellers, or compressors — one needs to understand the mechanisms of noise generation in these technical systems. Consequently one can optimize the device's geometry not only with respect to performance, but also with respect to noise. Often simulations are conducted in order to obtain a better understanding of noise generation, since measurements are difficult to carry out. There have been approaches to simulate the generated noise only in the static part of a device, and to account for the sound in the rotating part solely through the compressible flow computation [1]. However, such an approach needs a highly accurate flow computation to resolve the acoustic scales. In addition, the interaction of the acoustic field between the fixed and the rotating part may not be correctly taken into account.

Our approach is different in that we compute sound propagation in the whole system based on sound sources computed from a compressible flow solution using Lighthill's analogy. In this way we can study the mechanism of noise propagation in rotating parts, too. The coupling between the rotating and the fixed computational domain is realized on nonmatching finite element grids using a mortar method. This formulation has proven to work well for standard domains with fixed geometry [9]. The aim of this work is to show, that this method is also applicable for sound propagation in rotating systems.

2 Physical Problem

2.1 Aeroacoustic Analogy

For the computation of flow-induced noise we use Lighthill's inhomogeneous wave equation [6, 7] for the sound pressure $p_\sim$

$$\frac{1}{c_0^2}\frac{\partial^2 p_\sim}{\partial t^2} - \frac{\partial^2 p_\sim}{\partial x_i^2} = \frac{\partial^2 L_{ij}}{\partial x_i \partial x_j}. \tag{1}$$

The PDE is loaded on the right hand side by Lighthill's tensor

$$L_{ij} = \rho u_i u_j + ((p - p_0) - c_0^2(\rho - \rho_0))\delta_{ij} - \tau_{ij}, \tag{2}$$

which is calculated on the basis of data from a turbulent flow solution, that provides the density ρ, the particle velocity $\boldsymbol{u}$, the hydrodynamic pressure p, and the viscous stress tensor τ_{ij}. The mean values of density ρ_0, and pressure p_0, as well as the speed of sound c_0 are assumed to be given constants, and δ_{ij} denotes the Kronecker delta. The region of turbulent flow — called *source region* — can be kept quite small compared to the region of sound propagation. Outside of the source region Lighthill's tensor is set to zero, because here the disturbances in the fluid are solely due to acoustic waves.

In case of an isentropic flow at low Mach numbers, the source tensor may be further simplified. The viscous stress tensor τ_{ij} is responsible for the dissipation of acoustic energy into heat. This results in a damping over very large distances and is therefore neglected. The term $(p-p_0)-c_0^2(\rho-\rho_0)$ is only relevant for anisotropic media and can be assumed to be very small in air, compared to the first term of L_{ij}. Taking these simplifications into account, the source tensor is approximated by

$$L_{ij} \approx \rho u_i u_j. \tag{3}$$

A detailed discussion of our finite element formulation and its application to practical problems can be found in [5].

2.2 Rotating Formulation

Before we define a rotating acoustic system mathematically, we need to clarify, what physical meaning should be expressed by such a formulation. Strictly speaking, no ideally rotating volume of gas or fluid can exist, unless it is completely contained in a solid closed body, that is rotating itself. But since this case is irrelevant for technical applications, we need to make some simplifications. Assuming that the fluid volume inside an impeller or compressor is moving together with the rotating parts, sound propagation occurs with respect to the rotating frame of reference. Thus the computational domain is composed of a rotating region Ω_1, that couples to a surrounding stationary region Ω_2 at inflow and outflow boundary layers. This is clearly an extensive simplification, since we assume an exactly defined interface between moving and stationary fluid regions. In reality one would rather find a transition zone. On the other hand this is a similar assumption as used in sliding mesh techniques for computational fluid dynamics. So it is a natural choice to compute flow and sound propagation in the same frame.

Having in mind the discussion above, we are now ready to formulate the mathematical problem for the PDE defined by Eq. (1) and (3). Given an open bounded domain $\Omega := \Omega_1 \cup \Omega_2$ in $\mathbb{R}^2$ (depicted in Fig. 1), where the interface $\Gamma_I := \Omega_1 \cap \Omega_2$ is a circle with center $\mathbf{O}$. Let Γ_A denote the outer boundary of the domain. Analogously to [8] we define the rotation of Ω_1 by the ope-

rator $r_t : \Omega_1 \to \Omega_1$, which describes the rotation at time t by an angle $\theta = \omega t$, where ω is the circular speed of rotation. The reverse mapping is realized by the inverse operator r_{-t}. Then we may write the rotating region as a function of time

$$\Omega_1(t) = r_t \Omega_1(0). \tag{4}$$

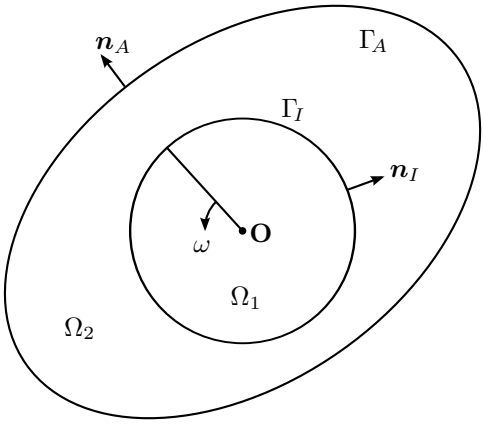

Figure 1: Sketch of the computational domain Ω

The unknown sound pressure is then split into a pair $p_\sim = (p_1, p_2)$, defined by the restriction of the unknown to the subdomains

$$p_k : \Omega_k \times [0, T) \to \mathbb{R}, \quad k = 1, 2. \tag{5}$$

On each subdomain Ω_k we define the unknown p_k in Lagrangian variables, i.e. each subdomain has its own frame of reference. In this way we avoid the presence of a convective term, but the movement is accounted for in time-dependent coupling conditions, that guarantee the continuity in the trace and flux of p_k (cf. Eq. (7) and (8)). On Γ_A an absorbing boundary condition is imposed (see Eq. (9)). The strong formulation of the problem reads:

Find p_1, p_2 such that

$$\frac{1}{c_0^2}\frac{\partial^2 p_k}{\partial t^2} - \frac{\partial^2 p_k}{\partial x_i^2} = \frac{\partial^2 L_{ij}}{\partial x_i \partial x_j} \qquad \text{in } \Omega_k,\ k = 1, 2, \tag{6}$$

$$p_1(r_{-t}\boldsymbol{x}, t) = p_2(\boldsymbol{x}, t) \qquad \text{on } \Gamma_I, \tag{7}$$

$$\frac{\partial p_1(r_{-t}\boldsymbol{x}, t)}{\partial \boldsymbol{n}_I} = \frac{\partial p_2(\boldsymbol{x}, t)}{\partial \boldsymbol{n}_I} \qquad \text{on } \Gamma_I, \tag{8}$$

$$\frac{\partial p_2}{\partial t} + c_0 \frac{\partial p_2}{\partial \boldsymbol{n}_A} = 0 \qquad \text{on } \Gamma_A, \tag{9}$$

$$p_k(\boldsymbol{x}, 0) = p_k^0 \qquad \text{in } \Omega_k,\ k = 1, 2, \tag{10}$$

where p_k^0 is a given initial condition, and $\boldsymbol{n}_A, \boldsymbol{n}_I$ are the outward normal unit vectors on Γ_A, Γ_I, respectively.

It is important to note, that this formulation only accounts for the movement of the fluid volume and the aeroacoustic sound sources contained in it. Refraction of sound waves in shear layers is not included explicitly in the formulation.

3 Finite Element Formulation

3.1 Weak Problem Formulation

In the following we omit the absorbing boundary and initial conditions for ease of presentation, and refer to [4] for details on this issue. The problem defined by Eq. (6)–(8) can be reformulated in a weak sense by making use of the functional space

$$T_k = \{f(\cdot, t) \mid f(\boldsymbol{x}, t) \in H^1,\, \boldsymbol{x} \in \Omega_k\}, \quad k = 1, 2, \tag{11}$$

where H^1 denotes the Sobolev space. The weak formulation is then obtained by multiplying Eq. (6) with test functions $w_k \in H^1$ and integrating over each subdomain Ω_k

$$\int_{\Omega_k} \frac{1}{c_0^2}\frac{\partial^2 p_k}{\partial t^2} w_k \,\mathrm{d}\Omega - \int_{\Omega_k} \frac{\partial^2 p_k}{\partial x_i^2} w_k \,\mathrm{d}\Omega = \int_{\Omega_k} \frac{\partial^2 L_{ij}}{\partial x_i \partial x_j} w_k \,\mathrm{d}\Omega, \quad k = 1, 2. \tag{12}$$

The above equation can be rewritten using Green's integral theorem [2], resulting in

$$\int_{\Omega_k} \frac{1}{c_0^2}\frac{\partial^2 p_k}{\partial t^2} w_k \,\mathrm{d}\Omega + \int_{\Omega_k} \frac{\partial p_k}{\partial x_i}\frac{\partial w_k}{\partial x_i} \,\mathrm{d}\Omega - \int_{\Gamma_I} \frac{\partial p_k}{\partial \boldsymbol{n}} w_k \,\mathrm{d}\Gamma = -\int_{\Omega_k} \frac{\partial w_k}{\partial x_i}\frac{\partial L_{ij}}{\partial x_j} \,\mathrm{d}\Omega, \quad k = 1, 2. \tag{13}$$

The interface conditions applied at Γ_I are realized by a mortar element method proposed by Flemisch et al. [3]. The coupling condition for the flux, defined in Eq. (8), is enforced in a strong sense by introducing the Lagrange multiplier

$$\lambda = -\frac{\partial p_1(r_{-t}\boldsymbol{x}, t)}{\partial \boldsymbol{n}_I} = -\frac{\partial p_2(\boldsymbol{x}, t)}{\partial \boldsymbol{n}_I}. \tag{14}$$

In contrast, the coupling condition for the trace (see Eq. (7)) is incorporated in a weak sense as

$$\int_{\Gamma_I} (p_1(r_{-t}\boldsymbol{x}, t) - p_2(\boldsymbol{x}, t))\mu \,\mathrm{d}\Gamma = 0, \tag{15}$$

with μ being a test function out of a suitable Lagrange multiplier space M_h, which will be defined later.

By inserting the definition of the Lagrange multiplier λ into the third term of Eq. (13), we arrive at the weak formulation of our problem.

Find p_1, p_2, λ such that

$$\sum_{k=1}^{2} \left(\int_{\Omega_k} \frac{1}{c_0^2}\frac{\partial^2 p_k}{\partial t^2} w_k \,\mathrm{d}\Omega + \int_{\Omega_k} \frac{\partial p_k}{\partial x_i}\frac{\partial w_k}{\partial x_i} \,\mathrm{d}\Omega \right) + \int_{\Gamma_I} (w_1 - w_2)\lambda \,\mathrm{d}\Gamma = -\sum_{k=1}^{2} \left(\int_{\Omega_k} \frac{\partial w_k}{\partial x_i}\frac{\partial L_{ij}}{\partial x_j} \,\mathrm{d}\Omega \right), \tag{16}$$

$$\int_{\Gamma_I} (p_1(r_{-t}\boldsymbol{x}, t) - p_2(\boldsymbol{x}, t))\mu \,\mathrm{d}\Gamma = 0, \tag{17}$$

for all μ, w_1, w_2.

3.2 Discretization

For the spatial discretization with finite elements we introduce triangulations $\mathcal{T}_k$ of the subdomains Ω_k, where the mesh size is denoted by $h_k = \max\{\mathrm{diam}(S) \,|\, S \in \mathcal{T}_k\}$, $k = 1, 2$. These triangulations are completely independent, i.e. in general $h_1 \neq h_2$ must be assumed, so that the triangulations are nonmatching at Γ_I.

For λ, μ the definition of a Lagrange multiplier space is required. We choose to define the Lagrange multiplier space as the space of continuous functions on the stationary side $\Gamma_I^2 := \mathcal{T}_2\big|_{\Gamma_I}$ of the interface

$$\lambda, \mu \in M_h := \left\{ g \in C^0(\Gamma_I^2) \right\}. \tag{18}$$

In nomenclature of the mortar methods, the rotating region Ω_1 is the *master* and the stationary region Ω_2 is the *slave*.

The unknowns p_1, p_2, λ are discretized on $\mathcal{T}_1, \mathcal{T}_2, \Gamma_I^2$ using nodal finite elements with a standard Lagrangian basis of first order. After the spatial discretization of Eq. (16) and (17) one may set up a semidiscrete system of the form

$$\begin{pmatrix} \mathbf{M}_1 & 0 & 0 \\ 0 & \mathbf{M}_2 & 0 \\ 0 & 0 & 0 \end{pmatrix} \begin{pmatrix} \ddot{p_1} \\ \ddot{p_2} \\ \ddot{\lambda} \end{pmatrix} + \\ + \begin{pmatrix} \mathbf{K}_1 & 0 & \mathbf{M} \\ 0 & \mathbf{K}_2 & \mathbf{D} \\ \mathbf{M}^{\mathrm{T}} & \mathbf{D}^{\mathrm{T}} & 0 \end{pmatrix} \begin{pmatrix} p_1 \\ p_2 \\ \lambda \end{pmatrix} = \begin{pmatrix} L_1 \\ L_2 \\ 0 \end{pmatrix}, \tag{19}$$

which is a symmetric saddle point problem. The coupling matrices are computed as [3]

$$[\mathbf{D}]_{pq} = \int_{\Gamma_I^2} N_{p,2}\, \phi_q \,\mathrm{d}\Gamma, \quad [\mathbf{M}]_{pq} = \int_{\Gamma_I} N_{p,1}\, \phi_q \,\mathrm{d}\Gamma, \tag{20}$$

where $N_{p,1}, N_{p,2}$ denote the nodal basis functions on the triangulations $\mathcal{T}_1, \mathcal{T}_2$, respectively, and ϕ_q is the nodal basis function of the Lagrange multiplier at node q. The calculation of $\mathbf{D}$ does not deviate from the standard finite element procedure, since both basis functions are defined on $\mathcal{T}_2$. Opposed to that, $\mathbf{M}$ requires special attention, because $N_{p,1}$ and ϕ_q are defined with respect to different grids. This issue will be addressed in the next section. Furthermore $\mathbf{M}$ has to be recomputed for each time step to account for the rotation of $\mathcal{T}_1$.

In order to obtain a fully discrete system, derivatives with respect to time are discretized by a second order implicit finite difference scheme of the Newmark family.

3.3 Implementation Details

The only open question left is, how to compute an integral of the form $\int N_{p,1}\, \phi_q \,\mathrm{d}\Gamma$? This is not obvious, because $N_{p,1}$ is defined on $\mathcal{T}_1$ and ϕ_q is defined on Γ_I^2. In case of planar interfaces, the integral is simply computed on the intersections of the master's elements with the slave's elements. This is not possible directly in our case. Since we are dealing with a circular interface, elements on both sides of the interface are not even collinear. A solution, commonly used in mortar methods, is to project an element of the master onto the plane of a slave element (Fig. 2(a)). The product of the basis functions is then computed on the intersection of the slave's element with the projection of the master's element. For the numerical evaluation of the integral, the integration points must be projected back onto the master element (Fig. 2(b)). Details on the latter two steps will be provided in the following.

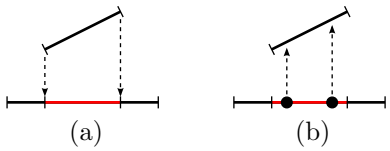

Figure 2: Treatment of the circular interface: projection of non-collinear elements (a), back-projection of integration points (b).

Note that this is one out of a variety of possible solutions. It is also possible to project the slave element onto the master side, or to project both elements onto an intermediate plane. The reason why we use the solution presented here is, that in this way we only have to recompute the coupling matrix $\mathbf{M}$ in each time step, while $\mathbf{D}$ has to be computed only once.

3.3.1 Intersection Calculation

Via an orthogonal projection of a master element onto a slave element, we receive two collinear line segments as input, given as the nodes of the master element's projection $[m_1', m_2']$ and the slave element $[s_1, s_2]$. The intersection calculation reduces in this case to an one-dimensional problem. For both nodes m_1', m_2' we calculate the local coordinates ξ_1, ξ_2 with respect to the slave element. Since we have no information about the direction of line segments, the local coordinates are then sorted, so that the relation $\xi_1 < \xi_2$ always holds. There are in total four cases (depicted in Fig. 3) that lead to an intersection:

1. $0 < \xi_1 < 1 \ \wedge \ \xi_2 \geq 1$:
   the intersection is the line $[m_1', s_2]$
2. $\xi_1 \leq 1 \ \wedge \ 0 < \xi_2 < 1$:
   the intersection is the line $[s_1, m_2']$
3. $\xi_1 \leq 0 \ \wedge \ \xi_2 \geq 1$:
   the intersection is the line $[s_1, s_2]$
4. $\xi_1 > 0 \ \wedge \ \xi_2 < 1$:
   the intersection is the line $[m_1', m_2']$

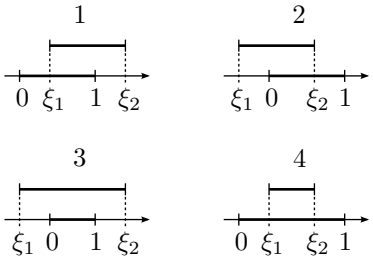

Figure 3: Four cases for the intersection of two collinear lines

3.3.2 Back-projection of Integration Points

Having applied the intersection algorithm described above, we are now ready to set up the coupling matrix $\mathbf{M}$. For numerical integration we use a Gaussian quadrature formula, which requires the evaluation of $N_{p,1}$ at certain integration points x_l. Since the integration points lie on the intersection element, we need to compute the back-projection $P^{-1}(x_l)$ onto the master element according to Fig. 4. First we compute the unit normal vectors of

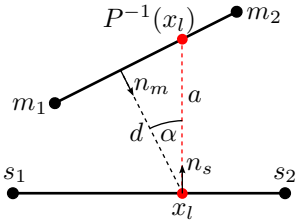

Figure 4: Back-projection of an integration point onto the master element

both the master and the slave element. Then we compute for each integration point its distance d to the master element. The unknown distance a is then computed via the relation

$$\cos\alpha = -n_m \cdot n_s = \frac{d}{a}. \tag{21}$$

Finally we get $P^{-1}(x_l)$ by scaling the normal vector n_s with a and adding it to the position vector x_l. In algebraic notation this algorithm reads:

m_i: nodes of the master element,
s_i: nodes of the slave element
x_l: global coordinate of l-th integration point
$n_m := \begin{pmatrix} m_{1y} - m_{0y} \\ m_{0x} - m_{1x} \end{pmatrix}$
$n_m := \frac{n_m}{|n_m|}$
$n_s := \begin{pmatrix} s_{1y} - s_{0y} \\ s_{0x} - s_{1x} \end{pmatrix}$
$n_s := \frac{n_s}{|n_s|}$
for all x_l **do**
  $d := |n_m \cdot (x_l - p_0)|$
  $P^{-1}(x_l) := x_l + \frac{d}{|n_m \cdot n_s|} n_s$
end for

4 Numerical Study

The verification of our method was performed for two test cases (sketched in Fig. 5). In both cases the outer boundary, on which absorbing boundary conditions are applied, is a circle with a diameter of 2 m. The rotating interface is a circle with a diameter of 1 m and is concentrical with the outer boundary. The difference between the two cases is the interior boundary:

1. a circle with center $(0, 0)$ and diameter 0.2 m,
2. a circle with center $(0.1\text{ m}, 0)$ and diameter 0.2 m.

In both cases, an artificial sine load at a frequency of 150 Hz is applied at the interior boundary in order to model an aeroacoustic source. Therewith we obtain for case 1 a fixed monopole source and for case 2 a rotating monopole source.

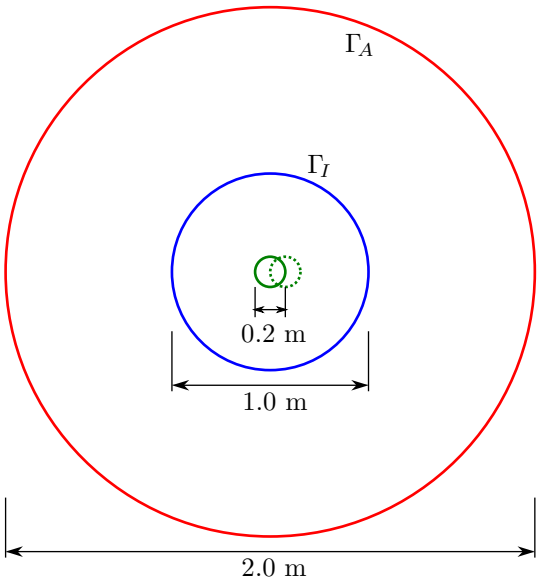

Figure 5: Sketch of the computational domain of two test cases: absorbing b.c. (Γ_A), interface (Γ_I), excitation in case 1 (solid green line), excitation in case 2 (dotted green line).

In order to avoid numerical errors, the discretization was chosen rather fine. In space a maximal element size of 5 cm was used, which corresponds to 45 linear finite elements per wavelength of the excitation and an angular resolution of 3°. The temporal excitation uses 40 time steps per period of the excitation, resulting in a time step of 0.167 ms. The interior domain rotates by an angle of 1° per time step, leading to a speed of 1000 rpm. Although the initial discretization is conforming at the interface, the situation is truly nonconforming, since the rotation leads to a step size that differs from the element size in axial direction.

For the first test case one would expect, that the rotation has no effect on the sound propagation, because the sound source is perfectly symmetric with respect to the axis of rotation. On the other hand, for test case 2 a change in amplitude and frequency is expected for different observation points. We pick out two locations, the topmost and the lowermost points of the domain, for which we want to validate the computed sound pressure. Fig. 7 shows that the numerical solution reflects the expected behavior. In the first case the sound pressure is identical in both locations, while in the second case the sound pressure clearly shows Doppler's effect. Furthermore, one can see in a contour plot of the sound pressure (Fig. 6) that the interface conditions work well, although the interface is placed in the near field ($\lambda \approx 2.27$ m).

5 Conclusions

In this contribution a finite element formulation for sound propagation in rotating systems was proposed. The initial approach was to decompose the computational domain into a rotating region and a fixed region, each of which has its own frame of reference. The coupling at

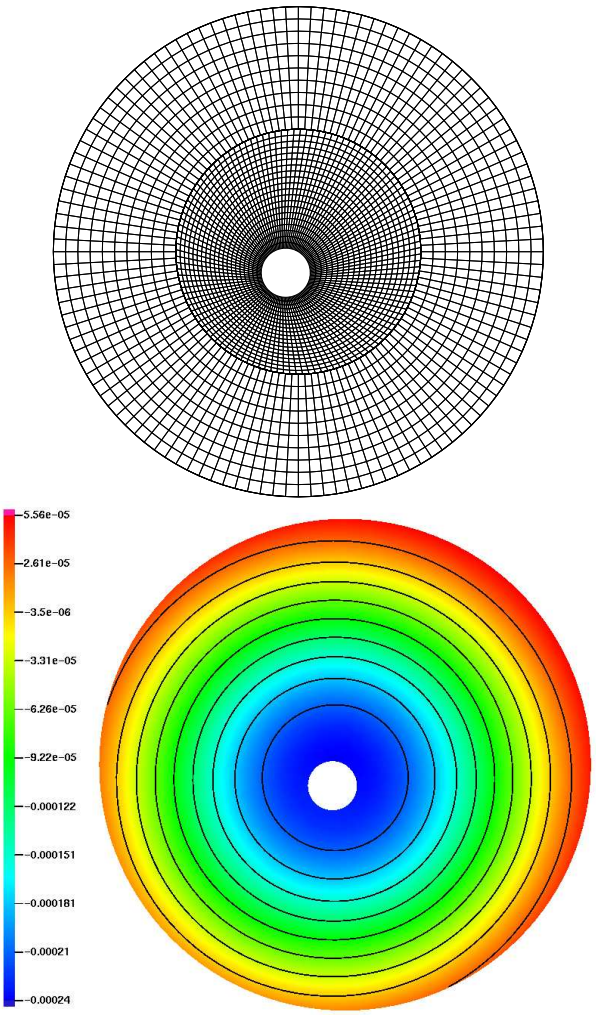

Figure 6: Snapshot of test case 2 at an angle of 240°: grid (top), solution (bottom)

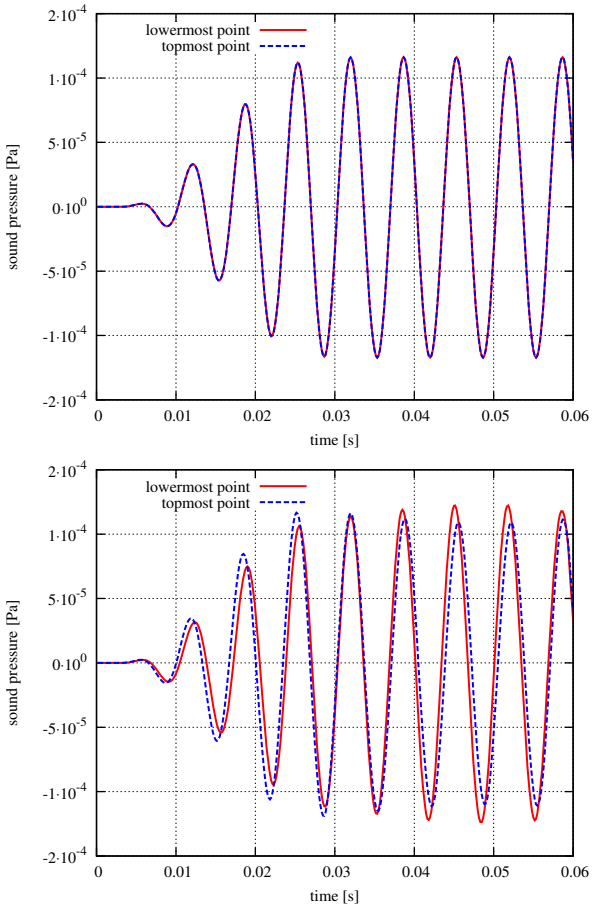

Figure 7: Comparison of solution at two points on the top and bottom boundary: quasistatic source (top), rotating source (bottom)

the interface between rotating and stationary region was enforced by a mortar method on nonmatching finite element grids. Numerical examples in two dimensions have shown that the method is stable and produces correct results. In the future it is desirable to extend the method to three dimensions, in order to apply it to technical devices.

References

[1] S. Caro, P. Ploumhans, X. Gallez, R. Sandboge, F. Shakib, M. Matthes, "A New CAA Formulation based on Lighthill's Analogy applied to an Idealized Automotive HVAC Blower using AcuSolve and Actran/LA", in *Proc. 11th AIAA/CEAS Aeroacoustics Conference, 23-25 May 2005, Monterey, CA, USA*, number 3015 in AIAA-2005 (2005)

[2] M. Escobar, *Finite Element Simulation of Flow-Induced Noise using Lighthill's Acoustic Analogy*, Ph.D. thesis, University of Erlangen-Nuremberg, Dept. of Sensor Technology, Erlangen, Germany (2007)

[3] B. Flemisch, M. Kaltenbacher, B. I. Wohlmuth, "Elasto-acoustic and acoustic-acoustic coupling on non-matching grids", *Int. J. Numer. Meth. Engng. 67*(13), 1791–1810 (2006)

[4] M. Kaltenbacher, *Numerical Simulation of Mechatronic Sensors and Actuators*, Springer-Verlag, Berlin Heidelberg New York, 2nd edition (2007)

[5] M. Kaltenbacher, M. Escobar, S. Becker, I. Ali, "Computational Aeroacoustics based on Lighthill's Acoustic Analogy", in S. Marburg, B. Nolte (eds.), *Computational Acoustics of Noise Propagation in Fluids*, chapter 4, 115–142, Springer-Verlag, Berlin Heidelberg (2008)

[6] M. J. Lighthill, "On Sound Generated Aerodynamically. I. General Theory", *Proc. Royal Society London A 211*(1107), 564–587 (1952)

[7] M. J. Lighthill, "On Sound Generated Aerodynamically: II. Turbulence as a Source of Sound", *Proc. Royal Society London A 222*(1148), 1–32 (1954)

[8] F. Rapetti, L. Santandrea, F. Bouillault, A. Razek, "Calculation of eddy currents in moving structures using a finite element method on non-matching grids", *COMPEL 19*(1), 10–29 (1999)

[9] S. Triebenbacher, M. Kaltenbacher, M. Meiler, H. Landes, "Enhanced Coupled Mechanical-Acoustic Field Computations on Nonmatching Grids", in *Proceedings of the Acoustics '08 Conference, 30 June - 4 July 2008, Paris* (2008)